Sensing Precision of an Optical Three-axis Tactile Sensor for a Robotic Finger

Masahiro Ohka, Hiroaki Kobayashi, Jumpei Takata and Yasunaga Mitsuya

Abstract—**We are developing an optical three-axis tactile sensor capable of acquiring normal and shearing force, with the aim of mounting it on a robotic finger. The tactile sensor is based on the principle of an optical waveguide-type tactile sensor, which is composed of an acrylic hemispherical dome, a light source, an array of rubber sensing elements, and a CCD camera. The sensing element of silicone rubber comprises one columnar feeler and eight conical feelers. The contact areas of the conical feelers, which maintain contact with the acrylic dome, detect the three-axis force applied to the tip of the sensing element. Normal and shearing forces are then calculated from integration and centroid displacement of the gray-scale value derived from the conical feeler's contacts. To evaluate the present tactile sensor, we have conducted a series of experiments using a *y-z* stage, a rotational stage, and a force gauge, and have found that although the relationship between the integrated gray-scale value and normal force depends on the sensor's latitude on the hemispherical surface, it is easy to modify the sensitivity according to the latitude, and that the centroid displacement of the gray-scale value is proportional to the shearing force. When we examined repeatability of the present tactile sensor with 1,000 load-unload cycles, the respective error of the normal and shearing forces was 2 and 5%.**

I. Introduction

Tactile sensors capable of sensing normal and shearing force produced on a robotic finger and an object are useful for fitting to a dextrose hand that can be applied to tasks that require human-like handling [1-17]. Examples include manufacturing tasks such as assembly, disassembly, inspection, and materials handing. We expect that demand for three-axis tactile sensors will grow with improvements in humanoid robot technology.

We have previously developed an optical three-axis tactile sensor based on the principle of an optical uni-axial tactile sensor comprising an optical waveguide plate, which is made of transparent acrylic and is illuminated along its edge by a light source [13-16]. The light directed into the plate remains within it due to the total internal reflection generated, since the plate is surrounded by air, which has a lower refractive index than the plate. A rubber sheet featuring an array of conical feelers is placed on the plate to keep the array surface in contact with the plate. If an object contacts the back of the rubber sheet, resulting in contact pressure, the feelers collapse, and at the points where these feelers collapse, light is diffusely reflected out of the reverse surface of the plate because the rubber has a higher refractive index than the plate. The distribution of contact pressure is calculated from the bright areas viewed from the plate's reverse surface.

It is possible to improve the uni-axial tactile sensor to design the three-axis tactile sensor. In the present study, which is based on previous investigations [18-21], we have developed a new sensing element for the three-axis tactile sensor that has a columnar feeler and eight conical feelers. The eight conical feelers maintain contact with the acrylic surface while the tip of the columnar feeler touches an object. Normal and shearing forces applied to the columnar feeler tip are calculated from the integrated gray-scale value and centroid displacement, respectively.

In the present study, we develop a hemispherical tactile sensor for general-purpose use with our three-axis tactile sensor, which we intend to mount on the fingertips of a multi-fingered hand. The present three-axis tactile sensor comprises an acrylic dome, a light source, an optical fiber scope, and a CCD camera. The light emitted from the light source is directed into the edge of the hemispherical acrylic dome through optical fibers. The sensing elements are arranged on the acrylic dome in a concentric configuration.

To evaluate the present tactile sensor, we have conducted a series of experiments using a loading machine that consists of a *y-z* stage, a rotational stage, and a force gauge. A normal force was applied to each sensing element that lined up along the meridian of the hemisphere to examine the dependence of sensing characteristics on the latitude. The shearing force component applied to the sensing element was generated by tilting the applied force against the sensing-element axis. We examined not only normal and shearing precision but also repeatability with the present three-axis tactile sensor.

II. Sensing Principle

Figure 1 shows a schematic view of the present tactile processing system to explain the sensing principle. The present tactile sensor is composed of a CCD camera, an acrylic board, a light source, and a computer. The light emitted from the light source is directed into the optical waveguide dome. The contact phenomena are observed as image data, which are acquired by the CCD camera and are

Manuscript received March 15, 2006.

Masahiro Ohka is with Graduate School of Information Science, Nagoya University, Furo-cho, Chikusa-ku, Nagoya, 464-8601, Japan (e-mail: ohka@is.nagoya-u.ac.jp).

Hiroaki Kobayashi, was with Graduate School of Engineering, Nagoya University, He is now with Toyota Industries Corporation, 2-1 Toyota-cho, Kariya, 488-8671.

Jumpei Takata is with Graduate School of Engineering, Nagoya University, Furo-cho, Chikusa-ku, Nagoya, 464-8603, Japan (e-mail: j_takata@nuem.nagoya-u.ac.jp).

Yasunaga Mitsuya is with Graduate School of Engineering, Nagoya University, He is a fellow of JSME, Furo-cho, Chikusa-ku, Nagoya, 464-8603, Japan (e-mail: mituya@nuem.nagoya-u.ac.jp).

transmitted to the computer to calculate the three-axis force distribution.

The sensing element presented in this paper comprises a columnar feeler and eight conical feelers as shown in Fig. 2. The sensing elements are made of silicone rubber, as shown in Fig. 1, and are designed to maintain contact with the conical feelers and the acrylic board and to make the columnar feelers touch an object. Each columnar feeler features a flange to fit the flange into a counter-bore portion in the fixing dome to protect the columnar feeler from horizontal displacement caused by shearing force.

When three components of force, the vectors F_x, F_y and F_z, are applied to the tip of the columnar feeler, contact between the acrylic board and the conical feelers is measured as a distribution of gray-scale values, which are transmitted to the computer. The F_x, F_y and F_z values are calculated using the integrated gray-scale value G and horizontal displacement of the centroid of the gray-scale distribution $\boldsymbol{u} = u_x \boldsymbol{i} + u_y \boldsymbol{j}$ as follows:

$$F_x = f(u_x), \quad (1)$$

$$F_y = f(u_y), \quad (2)$$

$$F_z = g(G), \quad (3)$$

where $\boldsymbol{i}$ and $\boldsymbol{j}$ are orthogonal base vectors of the x- and y-axes of a Cartesian coordinate, respectively; $f(x)$ and $g(x)$ are approximate curves estimated in calibration experiments.

III. Design of the Hemispherical Tactile Sensor

We are currently designing a multi-fingered robotic hand for general-purpose use in robotics. The robotic hand includes links, fingertips equipped with the three-axis tactile sensor, and micro-actuators (YR-KA01-A000, Yasukawa). Each micro-actuator consists of an AC servo-motor, a harmonic drive, and an incremental encoder, and is developed particularly for application to a multi-fingered hand.

Since the tactile sensors should be fitted to a multi-fingered hand, we are developing a fingertip to include a hemispherical three-axis tactile sensor. That is, the fingertip and the three-axis tactile sensor are united as shown in Fig. 3.

The sensing element of the tactile sensor is the same as the previously described element depicted in Fig. 2. The sensing elements are arranged on the acrylic dome in a concentric configuration. The acrylic dome is illuminated along its edge by optical fibers connected to a light source. Image data consisting of bright spots caused by the feelers' collapse are retrieved by an optical fiber-scope connected to the CCD camera.

IV. Experimental Conditions

A. Experimental apparatus

We have developed a loading machine as shown in Fig. 4. It includes an *x*-stage, a *z*-stage, rotary stages, and a force gauge (FGC-0.2B, NIDEC-SHIMPO Co.) to detect sensing characteristics of normal force and shearing force. The force gauge has a probe to measure force and can detect force in the range of from 0 to 2 N, with a resolution of 0.001 N. The positioning precisions of the *y*-stage, the *z*-stage, and the rotary stages are 0.001 mm, 0.1 mm, and 0.1 ° , respectively.

Output of the present tactile sensor is processed by the data processing system shown in Fig. 5. The system is composed of the tactile sensor, the loading machine, an

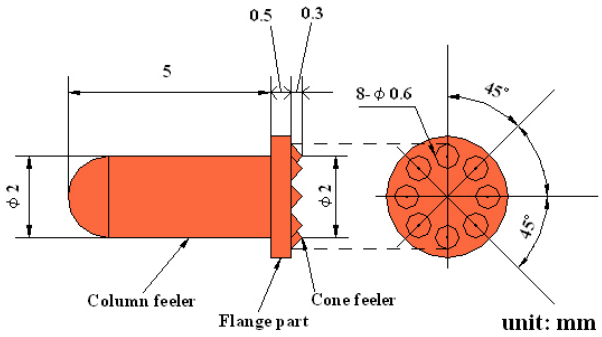

Fig. 2 Sensing element

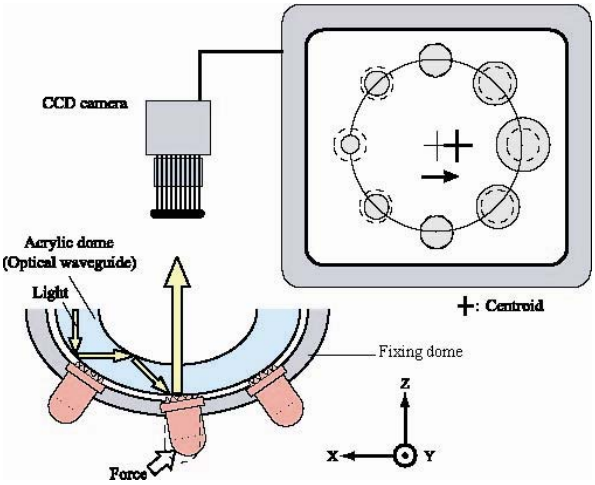

Fig. 1 Principle of the three-axis tactile sensor system

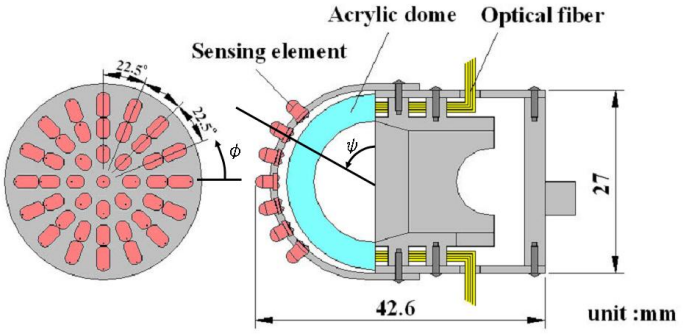

Fig. 3 Fingertip including the three-axis tactile sensor

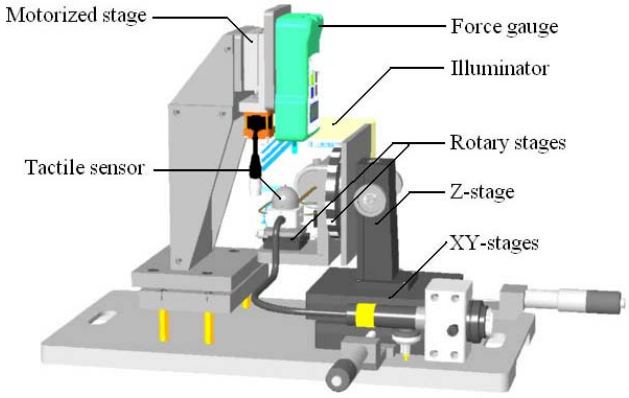

Fig. 4 Loading machine

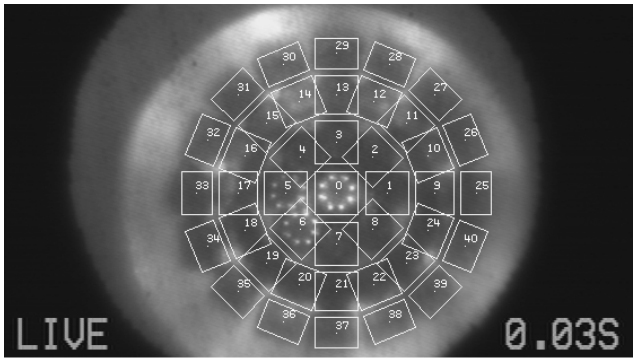

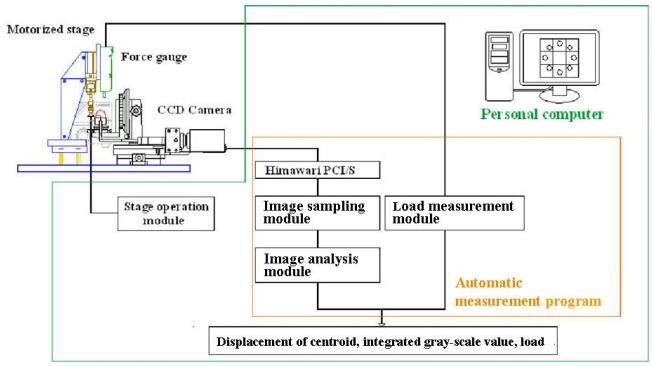

Fig. 5 Tactile data processing system

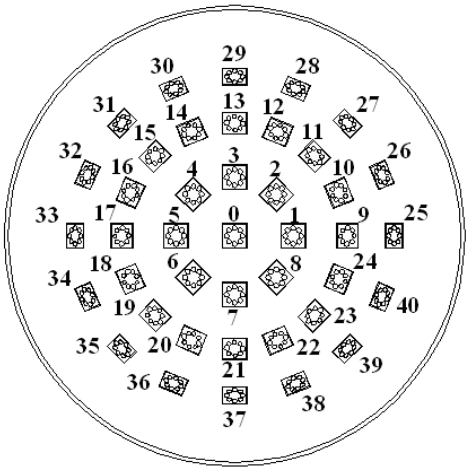

Fig. 6 Address of sensing elements

image-processing board (Himawari PCI/S, Library, Co.) and a computer. Image data acquired by the image processing board processed by software made in house.

Image data acquired by the CCD camera are divided into 41 sub-regions as shown in Fig. 6. The dividing procedure, digital filtering, integrated gray-scale value and centroid displacement are controlled on the image-processing board. Since the image warps due to projection from a hemispherical surface as shown in Fig. 6, software installed on the computer modifies the obtained data. The motorized stage and the force gauge are controlled by the software.

B. Sensing normal force

Because the present tactile sensor can detect not only normal force but also shearing force, we should confirm the sensing capability for both of these forces. In normal-force testing, by applying a normal force to the tip of a sensing element using the *z*-stage after rotating the attitude of the tactile sensor, it is easy to test the specified sensing element using the rotary stage. Since the rotary stage's center of rotation coincides with the center of the present tactile sensor's hemispherical dome, it is easy to test any sensing element aligned along the hemisphere's meridian.

C. Sensing shearing force

When we want to generate the shearing-force component, both the rotary stage and the *x*-stage are controlled in a way to specify the force direction and sensing element. At first, the rotary stage is operated to give the force direction θ as shown in Fig. 7. The *x*-stage is then tuned to the applied tilted force at the tip of the specified sensing element. Figure 7 shows that the sensing element located on the parietal region can be assigned according to the procedure described above. After that, a force is loaded onto the tip of the sensing element using the *z*-stage. Regarding the manner of loading, since the force direction does not coincide with the axis of the sensing element, slippage between the probe and the tip of sensing element occurs. To eliminate this problem, a spherical concave portion is formed on the probe surface to mate the concave portion with the hemispherical tip of the tactile element.

V. Experimental Results and Discussion

A. Sensing normal force

To evaluate the sensing characteristics of sensing elements distributed on the hemispherical dome, we need to measure the variation within the integrated gray-scale values generated by the sensor elements. Figure 8 shows examples

of variation in the integrated gray-scale value caused by increases in the normal force for sensors #00, #01, #05, #09, #17, #25 and #33. As the figure indicates, the gradient of the relationship between the integrated gray-scale value and applied force increases with an increase in θ; that is, the sensitivity depends upon the latitude on the hemisphere. Dome brightness is inhomogeneous because the edge of the dome is illuminated and light converges on the parietal region of the dome. The brightness is represented as a function of the latitude φ, and since the sensitivity is uniquely determined by the latitude, it is easy to modify the sensitivity according to φ.

However, sensing elements located at the same latitude φ show different sensing characteristics. For example, the sensitivities of #09 and #17 should coincide since they have the same latitude; however, as Fig. 8 clearly indicates, they do not. The difference is due to inhomogeneous brightness of the acrylic dome, as shown in Fig. 6. Therefore, we needed to obtain the sensitivity of every sensing element.

The relationship between the integrated gray-scale value and applied force has high repeatability. Experimental results from 1,000 repetitions on #00 are superimposed in Fig. 9, which shows that all the curves coincide with each. The deviation among them is within 2 %.

Normal force F_N and shearing force F_S applied to the sensing elements are calculated using the following formulas.

$$F_N = F_z \cos\theta \quad (4)$$

$$F_S = F_z \sin\theta \quad (5)$$

With Eq. (4) we obtained the variation in the integrated gray-scale values and applied normal force. Figure 10 displays the relationship for #00. Even if the inclination is varied from -30° to 30°, the relationship coincides within a deviation of 3.7 %.

As shown in Fig. 10, the relationship between the integrated gray-scale value and applied normal force is not completely linear; we approximate these curves as bi-linear, as shown in Fig. 11. The coefficients obtained for every sensing element are shown in Table 1 of the Appendix.

B. Sensing shearing force

When force is applied to the tip of the sensing element located in the parietal region under several θs, relationships between the displacement of the centroid and the shearing-force component calculated by Eq. (5) are obtained as shown in Fig. 12. Although the inclination of the applied

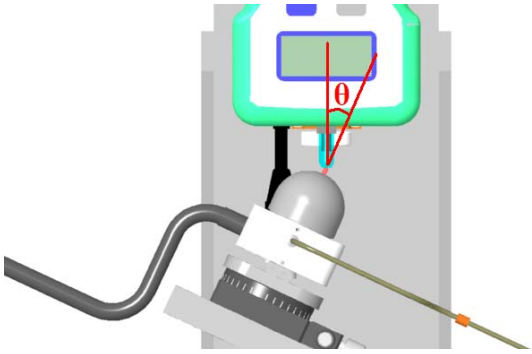

Fig. 7 Generation of shearing force component

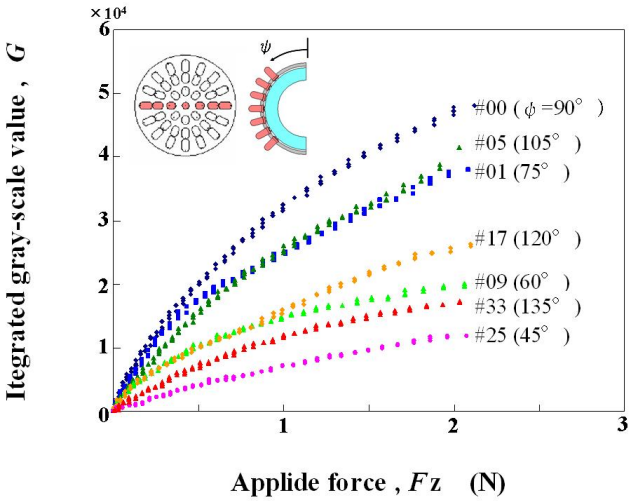

Fig. 8 Relationship between applied force and gray-scale value

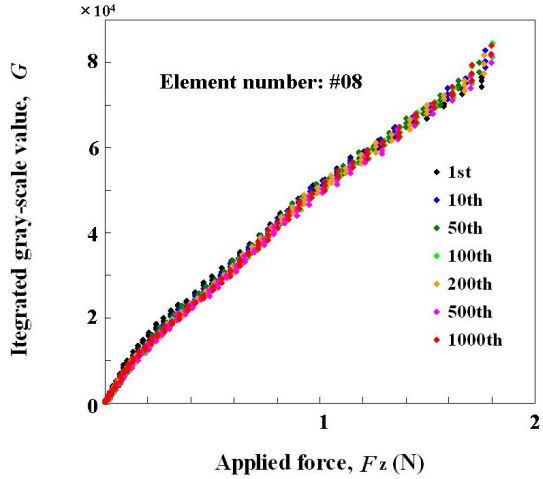

Fig. 9 Repeatability of relationship between integrated gray-scale value and applied force

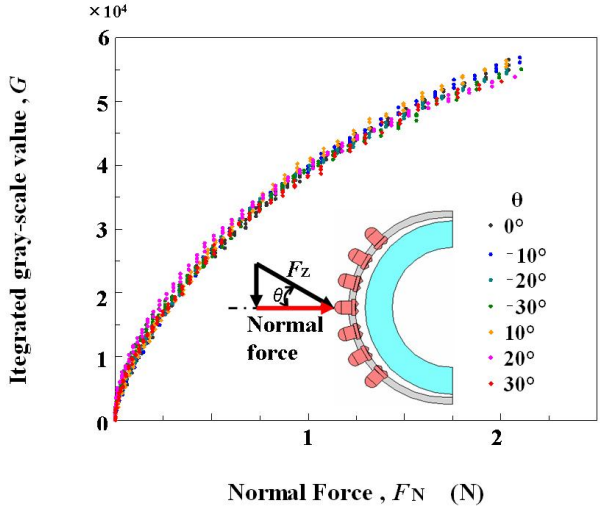

Fig. 10 Relationship between integrated gray-scale value and applied normal force at several inclinations

force is varied in the range from 15° to 60°, the curves converge into a single one. Therefore, the applied shearing force is obtained independently from displacement of the centroid. Since these relationships show bi-linear variation as well, we obtain can coefficients of every sensing element, which are given in Table 2 of the Appendix.

The bi-linear curve mentioned above was modified, taking into account the effect of friction between the acrylic dome and the conical feeler, to obtain the modified curves depicted in Fig. 13. Just as in Fig. 9, we performed 1,000 cyclic loadings to the tip of sensing element #00. Obtained curves are superimposed in Fig. 12. Again, all curves coincide with each other as shown in Fig. 13, and their deviation is less than 5%. The extent of deviation is rather higher that for normal force. It appears that the centroid is more easily disturbed and displaced by a slight change in loading direction than the integrated gray-scale value even if the probe tip has the concave portion mating with the tip of the sensing element. Therefore, we are convinced that repeatability results for the present sensor indicate that it is sufficiently sensitive to shearing force.

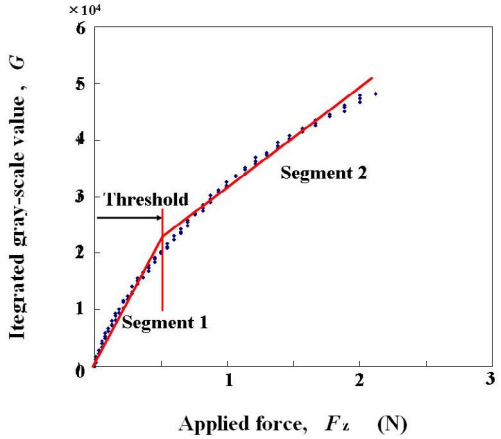

Fig. 11 Approximation using bi-linearity

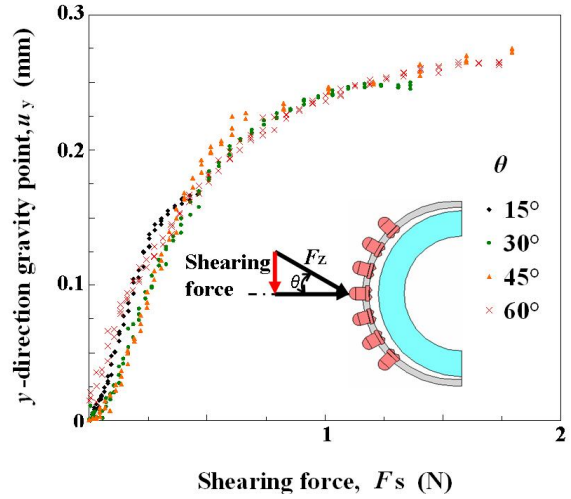

Fig. 12 Relationship between displacement of centroid and applied shearing force

VI. Conclusion

We have developed a new three-axis tactile sensor for mounting on multi-fingered hands, based on the principle of an optical waveguide-type tactile sensor comprising an acrylic hemispherical dome, a light source, an array of rubber sensing elements, and a CCD camera. The sensing element of the present tactile sensor includes one columnar feeler and eight conical feelers. A three-axis force applied to the tip of the sensing element is detected by the contact areas of the conical feelers, which maintain contact with the acrylic dome. Normal and shearing forces are calculated from integration and centroid displacement of the gray-scale value derived from the conical feeler's contacts.

To evaluate the present tactile sensor, we conducted a series of experiments using a *y-z* stage, rotational stages, and a force gauge. Although the relationship between the integrated gray-scale value and normal force depended on the sensor's latitude on the hemispherical surface, it was easy to modify the sensitivity according to the latitude. The sensitivity to normal force and shearing force were approximated with bi-linear curves. The results revealed that the relationship between the integrated gray-scale value and normal force converges into a single curve despite the inclination of the applied force. This was also true for the relationship between centroid displacement and shearing force. Therefore, applied normal and shearing forces can be obtained independently from the integrated gray-scale values and centroid displacement, respectively. Also, the results for the present sensor had enough repeatability to indicate that the sensor is sufficiently sensitive to both normal and shearing forces.

In future work, we plan to mount the present tactile sensor on a robotic finger to perform verification experiments. In the experiment, we will perform edge tracing of an object and object manipulation.

References

[1] Raibert, H.M. and Tanner, J.E., "Design and Implementation of a VSLI Tactile Sensing Computer," Int. J. Robotics Res., Vol. 1-3(1982), pp. 3-18.

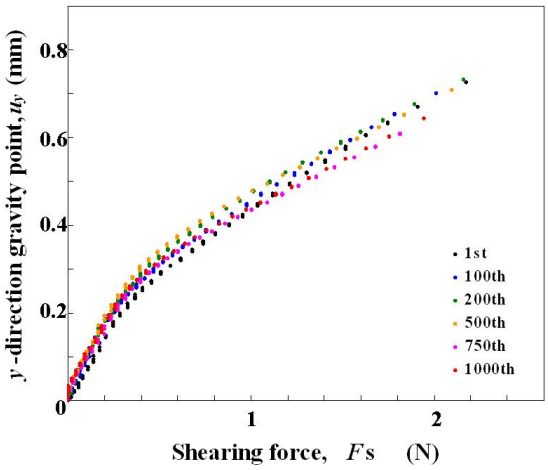

Fig. 13 Repeatability of relationship between displacement of centroid and applied shearing force

[2] Hackwood, S., Beni, G., Hornak, L. A., Wolfe, R. and Nelson, T. J., "Torque-Sensitive Tactile Array for Robotics," Int. J. Robotics Research, Vol. 2-2 (1983), pp. 46-50.
[3] Dario, P., Rossi, D.D., Domenci, C. and Francesconi, R., "Ferroelectric Polymer Tactile Sensors with Anthopomorphic Features," Proc. 1984 IEEE Int. Conf. On Robotics and Automation, (1984), pp. 332-340.
[4] Novak, J. L., "Initial Design and Analysis of a Capacitive Sensor for Shear and Normal Force Measurement," Proc. of 1989 IEEE Int. Conf. On Robotic and Automation, (1989), pp. 137-145.
[5] Hakozaki, M. and Shinoda, H., "Digital Tactile Sensing Elements Communicating Through Conductive Skin Layers," Proc. of 2002 IEEE Int. Conf. On Robotics and Automation, 2002, pp. 3813-3817.
[6] Yamada, Y. and Cutkosky, R., "Tactile Sensor with 3-Axis Force and Vibration Sensing Function and Its Application to Detect Rotational Slip," Proc. of 1994 IEEE Int. Conf. On Robotics and Automation, 1994, pp. 3550-3557.
[7] Nicholls, H. R. & Lee, M. H., "A Survey of Robot Tactile Sensing Technology," Int. J. Robotics Res., Vol. 8-3, (1989), pp. 3-30.
[8] Bicchi, A., Salisbury, J. K. and Dario, P., "Augmentation of Grasp Robustness Using Intrinsic Tactile Sensing," Proc. of 1989 IEEE Int. Conf. On Robotics and Automation, 1989, pp. 303-307.
[9] Howe, R. D. and Cutkosky M. R., "Dynamic Tactile Sensing: Perception of Fine Surface Features with Stress Rate Sensing," IEEE Trans on Robotics and Automation, Vol. 9, No. 2, (1993), pp. 140-151.
[10] Ohka, M. et al., "Tactile Expert System Using a Parallel-fingered Hand Fitted with Three-axis Tactile Sensors," JSME Int. J., Series C, Vol. 37, No. 1, 1994, pp. 138-146.
[11] Takeuchi, S., Ohka, M. and Mitsuya, Y., "Tactile Recognition Using Fuzzy Production Rules and Fuzzy Relations for Processing Image Data from Three-dimensional Tactile Sensors Mounted on a Robot Hand," *Proc. of the Asian Control Conf*., Vol. 3, 1994, pp. 631-634.
[12] Borovac, B., Nagy, L. and Sabli, M., "Contact Tasks Realization by sensing Contact Forces, Theory and Practice of Robots and Manipulators," Proc. of 11th CISM-IFToNN Symposium, Springer Wien New York, (1996), pp. 381-388.
[13] Mott, H., Lee, M. H. and Nicholls, H. R., "An Experimental Very-High-Resolution Tactile Sensor Array," in Proc. 4th Int. Conf. On Robot Vision and Sensory Control, pp. 241-250, 1984.
[14] Tanie, K., Komoriya, K., Kaneko M., Tachi, S. and Fujiwara, A., "A High-Resolution Tactile Sensor Array," Robot Sensors Vol. 2: Tactile and Non-Vision, Kempston, UK: IFS (Pubs), pp. 189-198, 1986.
[15] Nicholls, H. R., "Tactile Sensing Using an Optical Transduction Method," Traditional and Non-traditional Robot Sensors (Edited by T. C. Henderson), Springer-Verlag, pp. 83-99, 1990.
[16] Maekawa, H., Tanie, K., Komoriya, K., Kaneko M., Horiguchi, C. and Sugawara, T., "Development of a Finger-shaped Tactile Sensor and Its Evaluation by Active Touch," in Proc. of the 1992 IEEE Int. Conf. on Robotics and Automation, pp. 1327-1334, 1992.
[17] Hosoda, K., Tada, Y. and Asada, M., "Anthropomorphic Robotic Soft Fingertip with Randomly Distributed Receptors", Robotic and Autonomous Systems, vol. 54, pp. 104-109, 2006.
[18] Ohka, M. ,Mitsuya, Y., Takeuchi, S., Ishihara, H. and Kamekawa, O., "A Three-axis Optical Tactile Sensor (FEM Contact Analyses and Sensing Experiments Using a Large-sized Tactile Sensor)," in Proc. of the 1995 IEEE Int. Conf. on Robotics and Automation, pp. 817-824, 1995.
[19] Ohka, M., Mitsuya, Y., Matsunaga, Y. and Takeuchi, S., "Sensing Characteristics of an Optical Three-axis Tactile Sensor Under Combined Loading," Robotica, vol. 22, pp. 213-221, 2004.
[20] Ohka, M., Kawamura, T., Itahashi, T., Miyaoka, T. and Mitsuya, Y., "A Tactile Recognition System Mimicking Human Mechanism for Recognizing Surface Roughness," JSME International Journal, Series C. Vol. 48, No. 2, pp. 278-285, 2005.
[21] Ohka, M., Mitsuya, Y., Higashioka, I. and Kabeshita, H., "An Experimental Optical Three-axis Tactile Sensor for Micro-robots," Robotica, vol. 23, pp. 457-465, 2005.

Table 1 Coefficients for normal force sensing

No.	Threshold (N)	Segment 1		Segment 2	
		R^2	Sensitivity $\times 10^4$ (1/N)	R^2	Sensitivity $\times 10^4$ (1/N)
00	0.504	0.981	3.83	0.979	1.78
01	0.538	0.978	3.39	0.995	1.33
02	0.544	0.982	2.76	0.997	1.19
03	0.517	0.986	2.87	0.997	1.56
04	0.223	0.978	3.98	0.987	1.57
05	0.270	0.985	3.27	0.989	1.72
06	0.526	0.979	3.11	0.988	1.78
07	0.168	0.965	7.03	0.991	2.21
08	0.241	0.976	3.70	0.981	1.87
09	0.513	0.972	1.93	0.971	0.61
10	0.230	0.967	1.68	0.989	0.88
11	0.542	0.974	1.43	0.986	0.77
12	0.000	0.993	1.05	-	
13	0.095	0.997	2.58	0.992	0.96
14	0.163	0.928	3.08	0.996	0.98
15	1.069	0.961	1.36	0.964	0.63
16	0.515	0.981	2.31	0.988	1.31
17	0.269	0.958	2.39	0.993	1.11
18	0.282	0.974	3.08	0.974	1.65
19	0.531	0.987	2.17	0.980	1.38
20	0.528	0.990	2.51	0.976	1.34
21	0.513	0.983	2.95	0.987	1.24
22	0.509	0.974	3.18	0.978	1.16
23	0.314	0.978	3.58	0.984	1.15
24	0.546	0.980	1.95	0.990	1.01
25	0.613	0.987	0.79	0.991	0.52
26	0.183	0.965	1.47	0.982	0.41
27	0.208	0.955	1.66	0.974	0.50
28	0.251	0.911	1.07	0.990	0.45
29	0.000	0.982	0.63	-	
30	0.510	0.963	1.26	0.981	0.48
31	0.520	0.970	1.23	0.991	0.52
32	0.235	0.939	1.51	0.984	0.55
33	0.256	0.961	1.60	0.992	0.75
34	0.262	0.984	1.60	0.990	0.79
35	0.189	0.987	1.93	0.987	1.03
36	0.509	0.971	1.51	0.976	0.67
37	0.233	0.966	1.82	0.963	1.05
38	0.643	0.964	1.16	0.978	0.56
39	0.536	0.994	1.85	0.979	0.63
40	0.500	0.988	1.59	0.972	0.73

Table 2 Coefficients for shearing force sensing (#00)

Directional	Threshold (N)	Segment 1		Segment 2	
		R^2	Sensitivity (mm/N)	R^2	Sensitivity (mm/N)
x	0.742	0.984	0.508	0.999	0.263
y	0.758	0.972	0.511	0.999	0.270